CHEMISTRY OF MATERIALS
Article

Chem. Mater. **2010,** *22,* 1107–1113 1107
DOI:10.1021/cm902137s

Hydrogen Production and Characterization of $MLaSrNb_2NiO_9$ (M = Na, Cs, H) Based Photocatalysts†

Weifeng Yao,*[,‡,∥] Cunping Huang,[§] and Jinhua Ye*[,‡]

[‡]*Photocatalytic Materials Center, National Institute for Materials Science, 1-2-1 Sengen, Tsukuba, Ibaraki 305-0047, Japan,* [§]*University of Central Florida, Florida Solar Energy Center, Cocoa, Florida 32922, and* [∥]*Current address: Department of Energy and Environmental Engineering, Shanghai University of Electric Power, 2103 Pingliang Road, Shanghai 200090, China.*

Received July 22, 2009. Revised Manuscript Received November 9, 2009

Novel photocatalysts $MLaSrNb_2NiO_9$ (M = Na, Cs, H) were prepared for H_2 evolution from an aqueous methanol solution under both UV and visible light (> 420 nm) irradiation. $CsLaSrNb_2NiO_9$ (CNO) with a 2D layered structure (similar to that of $CsCa_2Nb_3O_{10}$) shows a much higher activity than the $NaLaSrNb_2NiO_9$ (NNO) photocatalyst that consists of a 3D cubic perovskite crystal structure (ABO_3). Experimental results show that Cs ions in CNO can be replaced by protons using a 1.0 M HNO_3 solution, forming a new photocatalyst, $HLaSrNb_2NiO_9$ (HNO), whereas Na^+ in NNO cannot be exchanged by H^+ under the same conditions. Results show that partially exchanging Cs ions with protons significantly improves the photocatalytic activity of CNO-based photocatalyst. It is found that the higher activities of CNO and HNO compared with that of NNO are attributed to larger surface areas and the 2D layered structure.

1. Introduction

Recently, photocatalytic water splitting has received special attention, as it could potentially provide a clean and renewable resource for the production of hydrogen fuel.[1] However, as compared with the application of photocatalytic oxidation in the abatement of volatile of organic pollutions, water splitting into H_2 and O_2 requires a large positive Gibbs energy (ΔG^0 = 237 kJ/mol). This makes water splitting more difficult to achieve than the photocatalytic degradation of air pollutants. Recently, Sayama, Arakawa, and co-workers proposed an interesting Z-scheme concept for water splitting using a two-photon excitation process.[1g] This system consisted of a $Pt/SrTiO_3$:Cr,Ta photocatalyst for H_2 evolution and a WO_3 photocatalyst for O_2 evolution via an IO_3^-/I^- redox couple as sacrificial reagents. The mechanism of hydrogen production by a Z-scheme method over two photocatalysts can be written as

$$6H^+ + 6e^- \xrightarrow{Pt/SrTiO_3:Cr,\,Ta\,+\,h\nu} 3H_2$$

$$I^- + 6OH^- + 6h^+ \xrightarrow{Pt/SrTiO_3:Cr,\,Ta\,+\,h\nu} IO_3^- + 3H_2O$$

$$IO_3^- + 3H_2O + 6e^- \xrightarrow{WO_3\,+\,h\nu} I^- + 6OH^-$$

$$6OH^- + 6h^+ \xrightarrow{WO_3\,+\,h\nu} \frac{3}{2}O_2 + 3H_2O$$

To accomplish photochemical water splitting via the Z-scheme method, photocatalysts with higher activities for O_2 and H_2 evolution are indispensable. It should be pointed out that the development of any new photocatalyst, even when based on a sacrificial reagent, could enhance our understanding of searching for a highly efficient overall water splitting photocatalyst. Thus, developing novel active photocatalysts for hydrogen generation or oxygen generation using a sacrificial material is still of great interest.

Since the early 1970s,[2−7] a variety of active photocatalysts have been reported for water splitting or hydrogen

†Accepted as part of the 2010 "Materials Chemistry of Energy Conversion Special Issue".

*Corresponding author. E-mail: weefeng.yao@gmail.com (W.Y.); jinhua.ye@nims.go.jp (J.Y.).

(1) (a) Fujishima, A.; Honda, K. *Nature* **1972**, *238*, 37. (b) Hoffman, M. R.; Martin, S. T.; Choi, W.; Bahnemann, D. W. *Chem. Rev.* **1995**, *95*, 69. (c) Asahi, R.; Morikawa, T.; Ohwaki, T.; Aoki, K.; Taga, Y. *Science* **2001**, *293*(13), 269. (d) Zou, Z.; Ye, J.; Sayama, K.; Arakawa, H. *Nature* **2001**, *414*, 625. (e) Khan, S. U. M.; Al-Shahry, M.; Ingler, W. B. Jr. *Science* **2002**, *297*, 2243. (f) Maeda, K.; Teramura, K.; Lu, D.; Takata, T.; Saito, N.; Inoue, Y.; Domen, K. *Nature* **2006**, *440*, 295. (g) Sayama, K.; Mukasa, K.; Abe, R.; Abe, Y.; Arakawa, H. *Chem. Commun.* **2001**, *23*, 2416.
(2) (a) Lehn, J. -M.; Sauvage, J. -P.; Ziessel, R. *Nouv. J. Chim.* **1980**, *4*, 623. (b) Domen, K.; Kudo, A.; Onishi, T.; Kosugi, N.; Kuroda, H. *J. Phys. Chem.* **1986**, *90*, 292. (c) Domen, K.; Kudo, A.; Onishi, T. *J. Catal.* **1986**, *102*, 92.
(3) Kato, H.; Kobayashi, H.; Kudo, A. *J. Phys. Chem. B* **2002**, *106*, 12441.
(4) (a) Kato, H.; Kudo, A. *Chem. Phys. Lett.* **1998**, *295*, 487. (b) Kato, H.; Kudo, A. *J. Phys. Chem. B* **2001**, *105*, 4285. (c) Kato, H.; Asakura, K.; Kudo, A. *J. Am. Chem. Soc.* **2003**, *125*, 3082.
(5) (a) Domen, K.; Kudo, A.; Shibata, M.; Tanaka, A.; Maruya, K.; Onishi, T. *J. Chem. Soc. Chem. Commun.* **1986**, 1706. (b) Kudo, A.; Sayama, K.; Tanaka, A.; Asakura, K.; Domen, K.; Maruya, K.; Onishi, T. *J. Catal.* **1989**, *120*, 337. (c) Sayama, K.; Arakawa, H.; Domen, K. *Catal. Today* **1996**, *28*, 175.
(6) (a) Takata, T.; Shinohara, K.; Tanaka, A.; Hara, M.; Kondo, J. N.; Domen, K. *J. Photochem. Photobiol. A* **1997**, *106*, 45. (b) Takata, T.; Furumi, Y.; Shinohara, K.; Tanaka, A.; Hara, M.; Kondo, J. N.; Domen, K. *Chem. Mater.* **1997**, *9*, 1063.
(7) Yoshimura, J.; Ebina, Y.; Kondo, J.; Domen, K.; Tanaka, A. *J. Phys. Chem.* **1993**, *97*, 1970.

Published on Web 11/24/2009

production using sacrificial reagents. In particular, 2D layered photocatalysts have been the focus of research in this area because their negative perovskite-like layers are believed to facilitate the separation of photogenerated electron−hole pairs that leads to the high activity of the photocatalyst. Furthermore, the optimization of chemical composition and microstructure by means of ion exchange is a useful approach in designing novel and high efficiency 2D layered photocatalysts. However, most of the reported 2D layered photocatalysts were active only under UV light irradiation. It is noted that although the $RbPb_2Nb_3O_{10}$ photocatalyst showed visible-light-driven photocatalytic activity for H_2 evolution from aqueous methanol solutions, the H_2 evolution rate was rather low (4 μmol/h).[7] Until today, the development of both UV and visible light active 2D layered photocatalysts are still the focus in this field because of the advantage of the 2D layered structure.

Doping active UV-light-driven photocatalysts with 3D transition metals is an effective method for the synthesis of new visible-light-sensitive photocatalysts.[1,8] However, to the best of our knowledge, the ion doping method has not been used on 2D layered photocatalysts. It is of interest to examine whether new visible-light-driven layered perovskite oxides could be produced by doping extra 3d transition metals into the perovskite-like host layers of the 2D layered oxides. Recently, a new compound $CsLaSrNb_2NiO_9$ (CNO) was reported as a 2D layered structure similar to that of $CsCa_2Nb_3O_{10}$.[9] It is noteworthy that when the alkaline cation Cs in the oxide was substituted with the smaller Na ions, the crystal structure changed from the 2D layered structure to a 3D perovskite structure (ABO_3) as that of Pb_2MgWO_6. Both CNO and $NaLaSrNb_2NiO_9$ (NNO) contain large amounts of 3d transition metal Ni^{2+} ions, suggesting that they could potentially absorb visible light and exhibit visible-light-driven photocatalytic activity. A preliminary investigation of the photocatalytic properties of CNO was carried out earlier.[10] The objective of this paper is to study the preparation and photocatalytic activities of new NNO and HNO photocatalysts by substituting Cs^+ with Na^+ and H^+.

2. Experimenal Section

2.1. Photocatalyst Preparation. All of the initial reagents, Cs_2CO_3, Na_2CO_3, La_2O_3, $SrCO_3$, Nb_2O_5, and NiO, were used as received without further purification (Wako, 99.9% purity or higher). CNO and NNO were prepared according to the literature[9] the stoichiometric mixtures of the starting materials were ground and mixed thoroughly in an agate mortar. An excess amount of Cs_2CO_3 or Na_2CO_3 (40 mol %) was applied to compensate for the loss of Cs and Na volatilization. The well-mixed powders were calcined at 1300 °C for 10 h. The resulting powders were then collected and washed with distilled water and air-dried at room temperature. The composition of as-prepared CNO and NNO was confirmed by elemental analysis using the Inductively Coupled Plasma Spectrometry (ICP). The protonated derivative oxide, HNO, was obtained by leaching the CNO powders in an HNO_3 aqueous solution: two grams of as prepared CNO powders were dispersed in 200 mL of a 1.0 M HNO_3 aqueous solution and stirred at room temperature for 72 h. To determine whether or not Na^+ in NNO can be protonated, 2 g of NNO powder was treated with HNO_3 acid under the same conditions and the content of Na^+ in the NNO was then measured.

2.2. Photocatalyst Characterization. The structures of the prepared samples were confirmed by the X-ray diffraction pattern (JEOL JDX-3500 Tokyo, Japan). UV−vis diffuse reflectance spectra were recorded using a UV/vis spectrometer (UV-2500, Shimadzu) and were converted to absorption spectra by the standard Kubelka−Munk method. A field-emission scanning electron microscope (FE-SEM, JEOL-JSM 6500F) and a transmission electron microscope (TEM, JEOL JEM-2000FX), operated at 200 kV, together with selected area electron diffraction (SAED) were used to determine the microstructure of the photocatalyst powder sample. The specific surface areas were measured by the conventional Brunauer−Emmett−Teller (BET) method (Gemini 2360, Shimadzu). Raman spectrum measurements were performed using a laser Raman spectrophotometer (Jasco NRS-1000) at room temperature.

2.3. Photocatalytic Reactions. Photocatalytic reactions were carried out in a gas-closed-circulation system. Before light irradiation, 2.5 kPa Argon gas was introduced into the evacuated system. The photocatalytic activity of the photocatalyst under UV light irradiation was measured using an inner irradiation type Pyrex cell with a 400W high-pressure Hg lamp (RIKO 400HA). The photocatalytic reactions for hydrogen production under visible light irradiation ($\lambda > 420$ nm) were recorded in a side window Pyrex cell. The light source was a 300 W Xe arc lamp attached with a cutoff filter (HOYA, L42). The evolved gas was determined by gas chromatograph (Shimadzu GC-8A) equipped with a thermal conductivity detector, which was connected to the system with a circulating line. For photocatalytic H_2 production from aqueous CH_3OH solutions, Pt cocatalyst was loaded onto the surface of as prepared photocatalyst by an in situ photodeposition method. In detail, an aqueous solution containing an appropriate amount of $H_2PtCl_6.6H_2O$ was mixed into the reactant solution. Under light irradiation, the metallic Pt could be generated from the solution and deposited onto the surface of the photocatalysts. The photocatalytic O_2 evolutions were performed in an aqueous $Ce(SO_4)_2$ solution.

3. Results and Discussion

3.1. Materials Characterization. *3.1.1. Structural and Morphology Analysis.* The obtained powders were all well-crystallized and the elemental analysis results are shown in Table 1. The results show that as prepared CNO and NNO closely match theoretical compositions. It should be pointed out that although additional 40 mol % Cs_2CO_3 and Na_2CO_3 were used for the preparation of NNO and CNO, unreacted Cs_2CO_3 and Na_2CO_3 could be dissolved in water and separated from NNO and CNO samples. Consistent with the results reported by Gopalakrishnan et al.,[9] the XRD patterns of NNO can be indexed with a cubic perovskite structure (ABO_3) (a = 3.96 Å),

(8) (a) Ye, J. H.; Zou, Z. G. *J. Phys. Chem. Solids* **2005**, *66*, 266. (b) Yin, J.; Zou, Z. G.; Ye, J. H. *J. Phys. Chem. B.* **2003**, *107*, 61. (c) Yin, J.; Zou, Z. G.; Ye, J. H. *J. Phys. Chem. B.* **2003**, *107*, 4936. (d) Yao, W. F.; Ye, J. H. *J. Phys. Chem. B* **2006**, *110*(23), 11188.
(9) Gopalakrishnan, J.; Uma, S.; Vasanthacharya, N. Y.; Subbanna, G. N. *J. Am. Chem. Soc.* **1995**, *117*, 2353.
(10) Yao, W. F.; Ye, J. H. *Catal. Lett.* **2006**, *110*, 139.

Table 1. Chemical Compositions of As-Prepared $NaSrLaNb_2NiO_9$ and $CsSrLaNb_2NiO_9$ Photocatalysts

sample	Na or Cs (wt%)	Sr (wt%)	La (wt%)	Nb (wt%)	Ni (wt%)
$NaSrLaNb_2NiO_9$	Na: 3.6[a]	13.7	21.8	29.1	9.2
	Na: 3.6[b]	13.2	21.2	28.7	9.2
$CsSrLaNb_2NiO_9$	Cs: 17.8[a]	11.7	18.6	24.8	7.8
	Cs: 17.9[b]	10.4	18.5	25.3	8.3

[a] Calculated on the basis of the molecular formula. [b] ICP analytical results.

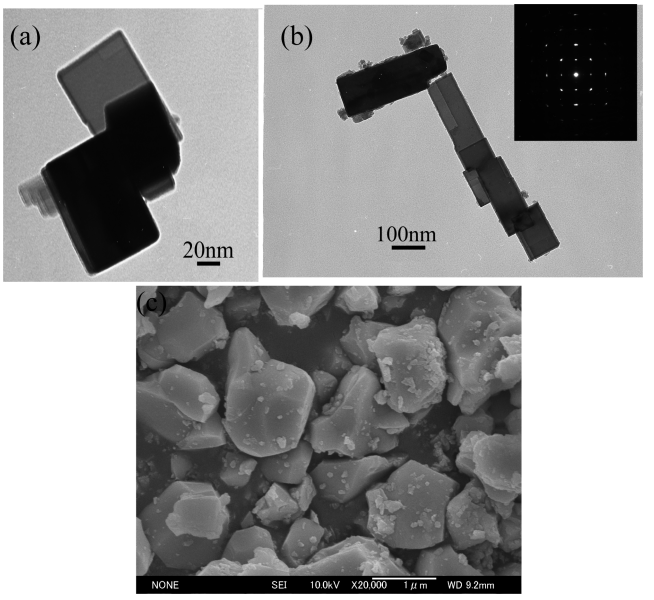

Figure 1. (a) TEM image of $CsLaSrNb_2NiO_9$; (b) TEM image and electron diffraction of $HLaSrNb_2NiO_9$; and (c) SEM image of $NaLaSrNb_2NiO_9$.

whereas CNO is a tetragonal cell (a = 3.97 Å, c = 22.5 Å) with a 2D-layered crystal structure that is similar to the structure of $CsCa_2Nb_3O_{10}$ or $CsSr_2Nb_3O_{10}$.[8,9] However, the structure of NNO was identified as $(NaLaSr)(Nb_2Ni)O_9$ with a 3D cubic ABO_3 perovskite crystal structure. The schematic crystal structures of CNO and NNO are shown in Figure S1 of the Supporting Information. Additionally, TEM images show that CNO consisted of tabular particles up to 0.3 μm in length (Figure 1a). As for NNO, the prepared powder sample consisted of large-sized particles (up to 1 μm) with irregular shapes (Figure 1c).

One of the important properties of the layered perovskite oxides is that the interlayer alkali metal ions can be replaced by protons in aqueous acidic solutions, forming a corresponding protonated derivative (i.e., $CsCa_2Nb_3O_{10}$ changes to $HCa_2Nb_3O_{10}$), which is a solid Bronsted acid that exhibits intracrystalline reactivity and intercalation behavior that is similar to that of clay minerals.[11] In this research, CNO was dispersed and stirred into a 200 mL of 1.0 M HNO_3 solution for 72 h. The Cs^+ in CNO can be partially exchanged with protons to produce protonated derivative $H_xCs_{1-x}LaSrNb_2NiO_9$.

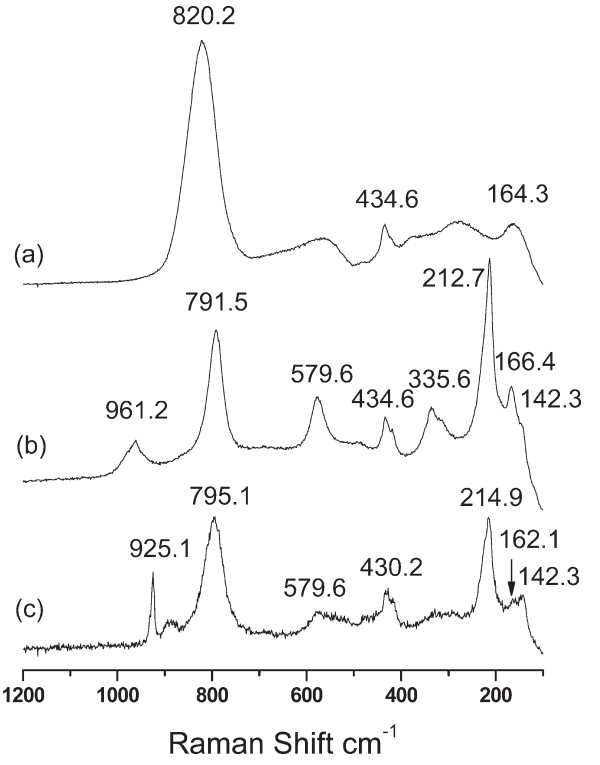

Figure 2. Raman spectra of as-prepared catalyst powders: (a) $NaLaSrNb_2NiO_9$, (b) $HLaSrNb_2NiO_9$, and (c) $CsLaSrNb_2NiO_9$.

For simplicity, we define it as $HLaSrNb_2NiO_9$ (HNO). On the other hand, however, Na^+ in NNO cannot be replaced by H^+ to form HNO under the same conditions. As shown in Figure S2 of the Supporting Information, the Raman spectra of NNO do not change before or after the acid treatment. However, the 925.1 cm^{-1} Raman absorption of CNO was shifted to 961.2 cm^{-1} (Figure 2). The TEM images and the orderly shaped SAED patterns suggested that as prepared HNO photocatalysts still maintained a good crystallinity (Figure 1b).

3.1.2. Raman Spectra of the Prepared Photocatalysts. Raman spectral features are sensitive to the crystal structure of the metal oxides. A slight structural change originating from the interaction between interlayers can affect the Raman spectra of a layered oxide. Figure 2 shows the Raman spectra of as prepared CNO, NNO, and HNO photocatalysts. The Raman spectrum of NNO shows three sharp peaks centered at 820.2, 434.6, and 164.3 cm^{-1}. The position of these Raman absorptions was found to be similar to those of other complex cubic perovskite oxides $A(B'_xB_{1-x})O_3$ (i.e., Pb_2MgWO_6).[12] In contrast, CNO shows a complicated Raman spectrum, which is similar to that of a typical 2D-layered oxide, $ACa_2Nb_3O_{10}$ (A = alkali metal).[13] According to the assignments of $ACa_2Nb_3O_{10}$ (A = alkali metal) Raman spectra, the sharp Raman band around 925.1 cm^{-1} of CNO can be attributed to the vibrational mode of the Nb−O terminal bond of the outer $Nb(Ni)O_6$ octahedra in CNO oxides.[9,13]

(11) Jacobson, A. J.; Lewandowski, J. T.; Johnson, J. W. *J. Less-Common Met.* **1986**, *116*, 137.

(12) Baldinozzi, G.; Sciau, P.; Bulou, A. *J.Phys.: Condens. Matter* **1995**, *7*, 8109.

(13) (a) Jehng, J.-M.; Wachs, I. E. *Chem. Mater.* **1991**, *3*, 100. (b) Byeon, S.-H.; Nam, H.-J. *Chem. Mater.* **2000**, *12*, 1771.

Note that no significant changes in Raman spectra were observed before or after acid treated CNO samples. However, the Raman absorption peak at 925.1 cm^{-1}, which was assigned to the terminal Nb−O bond, was shifted to 961.2 cm^{-1}. The terminal Nb−O bond is affected by neither the expansion of the perovskite layer nor by the change of interlayer space. It is also constant regardless of the identity of the alkali-metal layers.[13b] The shift in the Raman absorption spectrum of the terminal Nb−O bond was attributed to the substitution of alkali ions by the protons in the layered oxides. As mentioned previously, the alkali metal ions in its layered oxides can be replaced by protons. The interlayer proton is assumed to stabilize the terminal oxygen atoms by forming an −OH group interacting with the oxygen atom in the adjacent layer. This results in the shift of the Raman band.[13a] However, the major Raman absorption spectra of CNO remain unchanged, suggesting that the substitution of H^+ has little or no effect on the interlayer structure. In other words, HNO crystal structure maintains its layered structure in the CNO photocatalyst.

3.1.3. UV−Visible Absorption Spectra. All as prepared photocatalyst samples possess steep edges in their UV−visible absorption spectra. This indicates that the light response to NNO, CNO and HNO catalysts is not caused by impurity of donor levels but by a directed energy band gap from the valence band to the conduction band. The band gaps of NNO, CNO, and HNO were determined to be 2.84, 3.48, and 3.49 eV using the following equation

$$\alpha = A(h\nu - E_g)^{n/2}/h\nu$$

where α, h, ν, E_g, and A are absorption coefficient, Planck′s constant, light frequency, band gap, and a constant, respectively. The value of n was determined to be 1 for these catalysts from the UV−visible absorption spectra. As shown in the inset of Figure 3, three photocatalysts demonstrate the ability to absorb visible light, because a broad hump around 700 nm and a small hump from 387 to 455 nm appear in the UV−visible absorption spectra. Consistent with the different UV−visible diffuse reflectance spectra, the color of NNO is brilliant green, whereas CNO and HNO are grayish green. The band gap of a transition metal oxide was generally defined between the d level of the transition metal and the 2p level of the O atom.[14] However, when the oxides contain metals with the d orbital partially occupied, the electronic structure will be strongly influenced by those transition metals. The visible light response abilities of these oxides were assumed to be due to the splitting of the partially occupied Ni 3d orbitals in the octahedral field.[10] Further, the oxygen defects, formed in the photocatalysts when calcined at high temperature (1300 °C), could affect the formation of the broad absorption hump around 700 nm and the different background for these materials.

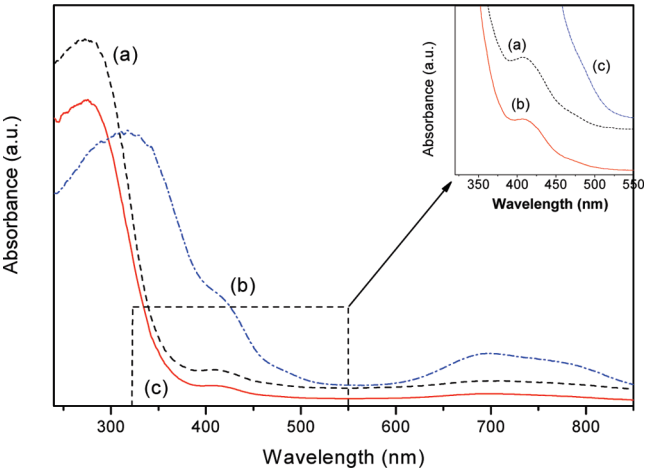

Figure 3. UV−visible absorption spectra for (a) $CsLaSrNb_2NiO_9$, (b) $NaLaSrNb_2NiO_9$, and (c) $HLaSrNb_2NiO_9$. Inset: The enlarged part of the UV−vis absorption spectra ranging from 320 to 550 nm.

3.2. Hydrogen Production from CNO-Based Photocatalysts. Hydrogen production activity of a photocatalyst is normally measured using methanol as a sacrificial reagent. The mechanism of hydrogen production from an aqueous methanol solution over photocatalysts can be written as

$$\text{photocatalyst} + h\nu \rightarrow \text{photocatalyst} + h^+ + e^-$$

$$2h^+ + CH_3OH \rightarrow CH_2O + 2H^+$$

$$4h^+ + CH_2O + H_2O \rightarrow CO_2 + 4H^+$$

$$6e^- + 6H^+ \rightarrow 3H_2\uparrow$$

The overall reaction for hydrogen evolution is $CH_3OH + H_2O \xrightarrow[h\nu]{\text{photocatalyst}} CO_2 + 3H_2\uparrow$ Figure 4a shows UV-light photocatalytic hydrogen production from an aqueous methanol solution in the presence of Pt loaded CNO photocatalyst (Pt/CNO). The rate of H_2 production was about 1242 μmol/(h $g_{catalyst}$) and it remained constant during the reaction. In contrast, the rates of H_2 evolution over other 2D layered photocatalysts, such as $KCa_2Nb_3O_{10}$, $CsCa_2Nb_3O_{10}$, $KSr_2Nb_3O_{10}$, and $K_xLa_{1-x}Ca_{1+x}Nb_3O_{10}$ (x = 0.25, 0.5, 0.75), were reported to be less than 215 μmol/(h $g_{catalyst}$) under similar conditions.[15] After evacuating the reaction system and rerunning the experiment, an almost identical gas production rate was achieved. Nearly 4000 μmol of H_2 were collected during a 6.5 h experiment. In this reaction, the molar ratio of the total hydrogen evolved to the photocatalyst (670 μmol) used is about 6. In terms of the reacted electrons relative to the amount of Pt loading on the surface of the photocatalysts, the turnover number exceeded 620. This indicates that the H_2 produced does result from a

(14) (a) Scaife, D. E. *Solar Energy* **1980**, *25*, 41. (b) Arima, T.; ToKura, Y. *Phys. Rev. B* **1993**, *48*, 17006.

(15) (a) Takata, T.; Tanaka, A.; Hara, M.; Kondo, J. N.; Domen, K. *Catal. Today* **1998**, *44*, 17. (b) Domen, K.; Ebina, Y.; Ikeda, S.; Tanaka, A.; Kondo, J. N.; Maruya, K. *Catal. Today* **1996**, *28*, 167.

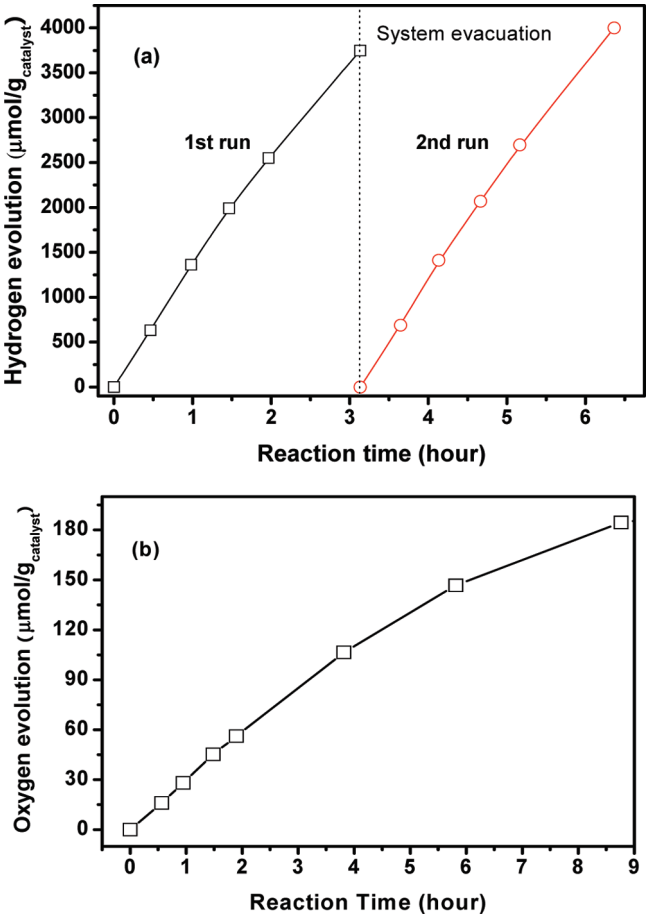

Figure 4. (a) Photocatalytic hydrogen production from an aqueous methanol solution. (Photocatalyst: 0.5 g of Pt (0.5 wt %)/$CsLaSrNb_2NiO_9$. Light source: 400 W high-pressure Hg lamp. Solution composition: 370 mL o 3.3 M CH_3OH aqueous solution) (b). Photocatalytic oxygen production from an aqueous cerium sulfate solution. (Photocatalyst: 0.5 g of $CsLaSrNb_2NiO_9$. Light source: 400 W high-pressure Hg lamp. Solution composition: 370 mL of 8.2 mM $Ce(SO_4)_2$ aqueous solution.).

photocatalytic reforming of CH_3OH rather than from decomposition of the photocatalyst. The XRD patterns of CNO supported this conclusion because they remained unchanged before and after H_2 production.

The photocatalytic activity of CNO-based photocatalyst for oxygen production was detected using $Ce(SO_4)_2$ as the sacrificial material (Figure 4b). The overall reaction for the oxygen production[16] is

$$4Ce^{4+} + 2H_2O \xrightarrow[h\nu]{\text{photocatalyst}} 4Ce^{3+} + O_2\uparrow + 4H^+$$

Figure 4b indicates that CNO based photocatalyst can serve as a water oxidation photocatalyst and show a long-term activity for photocatalytic O_2 production from an aqueous $Ce(SO_4)_2$ solution under UV-light irradiation. Similar results were also obtained when $AgNO_3$ was used as a sacrificial reagent. As shown in the Supporting Information, Figure S3, CNO shows a high activity for O_2 evolution from aqueous $AgNO_3$ solution under UV light irradiation. It should be pointed out that the decline

(16) Zhigang, Z.; Jinhua, Y.; Ryu, A.; Hironori, A. *Catal. Lett.* **2000**, *68*, 235.

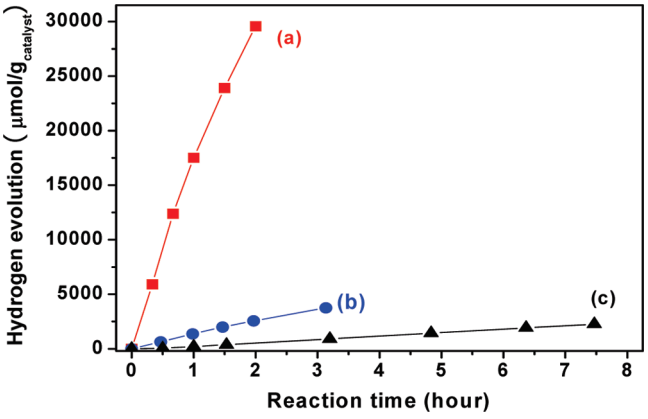

Figure 5. Hydrogen evolution from an aqueous methanol solution. Photocatalysts: (a). 0.2 g of Pt(0.5 wt %)/$HLaSrNb_2NiO_9$, (b) 0.5 g of Pt (0.5 wt %)/$CsLaSrNb_2NiO_9$, and (c) 0.5 g of Pt (0.5 wt %)/$NaLaSrNb_2NiO_9$. Light source: 400 W high-pressure Hg lamp. Solution composition: 370 mL of 3.3 M CH_3OH aqueous solution.

of the oxygen evolution rate in Figure S3 of the Supporting Information results from the light blockage effect when fine Ag particles are formed during the oxygen production process.

3.3. Effect of Na, Cs, and H Cations on the Photocatalytic Activities of $MLaSrNb_2NiO_9$-Based (M = Na, Cs, H) Photocatalysts. As mentioned previously, the crystal structure of $MLaSrNb_2NiO_9$ based photocatalysts is dependent on the alkaline cations in the M sites of $MLaSrNb_2NiO_9$. Cs ions occupy the M sites in CNO with a 2D layered perovskite structure that is similar to the structure of $CsSr_2Nb_3O_{10}$, whereas NNO with Na ions in the M sites shows a 3D-cubic perovskite structure similar to the structure of $A(B'_xB_{1-x})O_3$, such as Pb_2MgWO_6.[12] It is of interest to compare the photocatalytic activities of these oxides with similar compositions but different crystal structures. Figure 5 shows the effect of Na and Cs on the hydrogen production activities of $MLaSrNb_2NiO_9$-based (M = Na, Cs, H) photocatalysts. The hydrogen evolution rate of Pt/NNO (330 μmol/(h $g_{catalyst}$)) is much lower than the rate of 1242 μmol/(h $g_{catalyst}$) for Pt/CNO. One reason for the higher photocatlytic activity of the 2D layered crystal structure of CNO is that it possesses negative perovskite-like layers that facilitate the separation of photocatalytically generated electron−hole pairs.[5,6] The second reason is the larger surface area of CNO (6.1 m^2/g) as compared to 1.3 m^2/g of NNO (Table 2). A large surface area in a photocatalyst enhances its absorption of reactants and improves its photocatalytic activity.[17]

It is noted that a new-layered perovskite oxide HNO could be prepared by exchanging Cs^+ in CNO with H^+ from an acidic solution. However, HNO could not be synthesized by treating NNO with the same acid. Figure 5 shows that the rate of hydrogen evolution for the protonated CNO (HNO) is significantly increased, whereas the rate remains unchanged for acid-treated NNO photocatalyst. This result indicates that HNO exhibits a significantly improved hydrogen evolution rate (15 000 μmol/(h $g_{catalyst}$))

(17) Yao, W. F.; Iwai, H.; Ye, J. H. *Dalton Trans.* **2008**, 1426.

Table 2. Hydrogen Evolution Rates and the BET Surface Areas of $MLaSrNb_2NiO_9$ (M = Na,Cs,H) Photocatalysts

	rate of H_2 evolution		
composition	UV light irradiation[a] (μmol/(h $g_{catalyst}$))	visible light irradiation[b] (μmol/(h $g_{catalyst}$))	BET (m^2/g)
$NaLaSrNb_2NiO_9$	330		1.3
$CsLaSrNb_2NiO_9$	1242	0.6	6.1
$HLaSrNb_2NiO_9$	15000	3.0	26.7

[a] The light source is a 400 W high-pressure Hg lamp. [b] The light source is a 300 W Xe arc lamp attached with a cutoff filter (HOYA, L42) (λ > 420 nm).

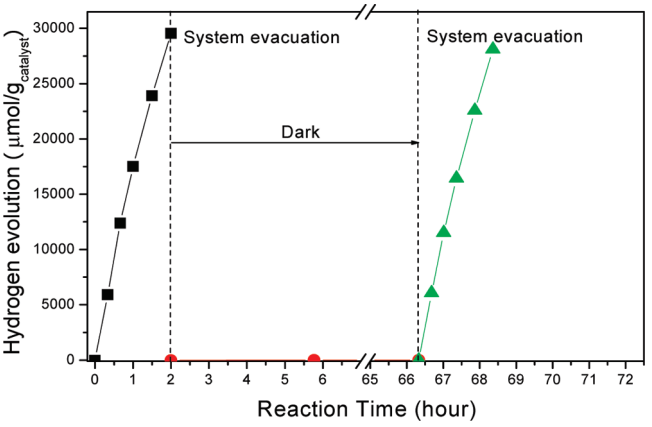

Figure 6. Hydrogen evolution from an aqueous methanol solution. (Photocatalysts: 0.2 g of Pt(0.5 wt %)/$HLaSrNb_2NiO_9$. Light source: 400 W high-pressure Hg lamp. Solution composition: 370 mL of 3.3 M CH_3OH aqueous solution).

in comparison with that of the CNO-based photocatalyst (1242 μmol/(h $g_{catalyst}$)). The quantum efficiency of hydrogen production over Pt/HNO photocatalyst, calculated using the following definition

$$\eta = \frac{\text{no. of electrons}}{\text{no. of irradiated photons}} = \frac{\text{no. of hydrogen atoms generated}}{\text{no. of irradiated photons}}$$

was 42.3% with the UV irradiation centered at 253.7 nm by a UV lamp (GL 15, 253.7 nm, Toshiba). XRD patterns that remain unchanged before and after the photocatalytic reactions suggest that HNO is a stable photocatalyst without occurrence of structural degradation during the reaction. Figure 6 shows that hydrogen evolution is a photodriven reaction. Hydrogen is produced over the photocatalyst with the UV light irradiation. After the lamp was turned off ,no H_2 evolution was detected for the next 60 h. Upon the lamp being turned on again, the H_2 evolution restarted and the rate approximated that of the first run. The large surface area (26.7 m^2/g) is an important reason attributed to the significant increase in the hydrogen production rate for HNO based photocatalyst. On the other hand, the reactant molecules, i.e., H_2O and CH_3OH, can be intercalated into the interlayer space of the protonated niobate layered oxides.[18]

(18) Ebina, Y.; Tanaka, A.; Kondo, J. N.; Domen, K. *Chem. Mater.* **1996**, *8*, 2534.

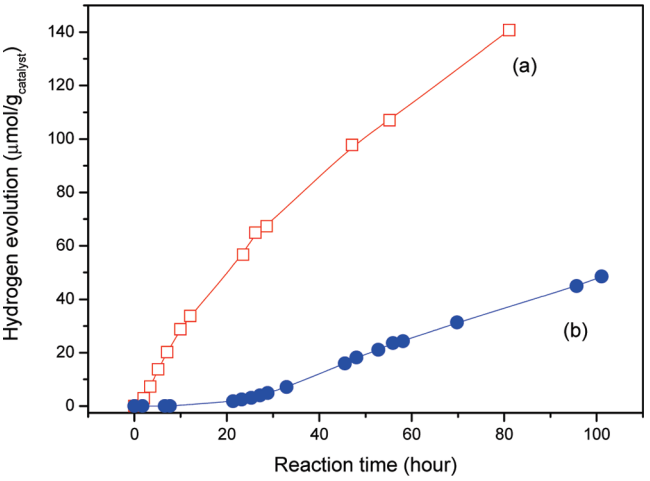

Figure 7. Visible-light photocatalytic hydrogen evolution from an aqueous methanol solution. (Photocatalysts: (a) 0.2 g of Pt-0.5 wt %/$HLaSrNb_2NiO_9$, (b) 0.5 g of Pt-0.5wt.%/$CsLaSrNb_2NiO_9$. Light source: 300 W Xe lamp with band filter (λ > 420 nm). Solution composition: 270 mL of 4.5 M CH_3OH aqueous solution.).

The migration of reactants into the interlayer space was assumed to promote the formation of protonated niobate oxides, facilitating the hydrogen production rate. This is due to the resulting decrease in the distance between photogenerated electrons or holes to reactants. For the unprotonated niobate layered oxides, however, the reactant molecules were hardly intercalated into the interlayer space because of the high charge density of the niobate layers.[18]

3.4. Visible-Light-Induced Activities of $MLaSrNb_2NiO_9$-Based (M = Na, Cs, H) Photocatalyst for Hydrogen Production. Similar to UV light photocatalytic hydrogen production, visible-light-induced photocatalyic hydrogen evolution was performed using CH_3OH as the sacrificial reagent. Figure 7 shows that hydrogen evolution over Pt/CNO photocatalyst requires at least 10 h of light irradiation. Further experiments showed that visible light photocatalytic hydrogen generation was detected immediately when light was on for the used Pt/CNO photocatalysts (after the reaction of H_2 evolution under UV light irradiation). The prolonged hydrogen evolution for the fresh CNO photocatalyst is attributed to the photoreduction of H_2PtCl_6 solution for the formation of metal Pt particles loaded onto the surface of the photocatalyst. In contrast, Figure 7 shows that the delayed hydrogen production does not apply to Pt/HNO photocatalyst. The hydrogen production rate of Pt/HNO is also much higher than that of Pt/CNO under visible light irradiation. As depicted in Figure 7, the rates of H_2 production are about 0.6 μmol/(h $g_{catalyst}$) and 3.0 μmol/(h $g_{catalyst}$) for Pt/CNO and Pt/HNO photocatalysts, respectively. The quantum efficienc of Pt/CNO and Pt/HNO photocatalysts are too low to measure under the visible light irradiation. As estimation based on the quantum efficiencies of the photocatalysts under UV light irradiation, the visible light quantum efficiencies of these materials were estimated to be lower than 1%. Although quantum efficiencies are low, our experimental results

show that that the visible light activities of H_2 production over Pt/CNO and Pt/HNO are stable over 100 h. The XRD patterns of the photocatalysts remained unchanged before and after the reaction, implying that the photocatalysts are stable for the photocatalytic reaction.

It should be pointed out that the electronic structure of the transition metal oxides with perovskite structure is generally defined by the d-level of the transition metal (such as Ti^{4+}, Nb^{5+}, and Ta^{5+}) and the 2p level of O atoms. However, for an oxide-containing transition metals with the d orbitals partially occupied, such as Ni^{2+} and Cr^{3+}, the electronic structure would be strongly influenced by these ions. Previous studies of Ni-doping on the photocatalytic properties of TiO_2 and $SrTiO_3$ photocatalysts have showed that an occupied level was created in the center of the band gap because of the Ni 3d band splitting in the oxides,[19] which promotes visible-light-driven photocatalytic activities of TiO_2 (3.2 eV) and $SrTiO_3$ (3.3 eV) catalysts. As for CNO and HNO photocatalysts, the crystal structure consists of perovskite-like slabs of composition [$LaSrNb_2NiO_9$] interleaved with the Cs or H cations.[9] The visible absorption ability of CNO and HNO catalysts was attributed to the band splitting of Ni 3d orbitals in the octahedral sites that form new band levels in the forbidden band of the photocatalysts.[10] Therefore, the visible light driven photocatalytic activity was influenced by the Ni ions, which are incorporated into the perovskite-like slabs [$LaSrNb_2NiO_9$] of CNO and HNO photocatalysts. In this paper, we reported for the first time a 2D layered photocatalyst and its protonated derivative oxide photocatalysts by incorporating 3d transition ions into the perovskite-like slabs to have activity under visible light irradiation. Considering the large number of 2D layered oxides and the advantages of the layered structure for photocatalytic hydrogen production, the novel structure with doping transitional metal ions into a 2D layered metal oxide may point to a new direction in seeking more efficient visible light active photocatalysts.

(19) Niishiro, R.; Kato, H.; Kudo, A. *Phys. Chem. Chem. Phys.* **2005**, *7*, 2241.

4. Conclusion

In summary, we have found hydrogen and oxygen production activities from novel $MLaSrNb_2NiO_9$-based (M = Na, Cs, H) photocatalysts. The 2D layered photocatalysts, $CsLaSrNb_2NiO_9$ (CNO) and $HLaSrNb_2NiO_9$ (HNO), demonstrate hydrogen production under visible light irradiation (420 nm). Under UV-light irradiation, CNO and HNO photocatalysts show much higher hydrogen evolution rates than that of $NaLaSrNb_2NiO_9$ (NNO). The characterization of the photocatalysts shows that the higher hydrogen production rate is attributable to the large surface areas of the photocatalysts and the 2D layered structure that facilitates the separation of photogenerated electrons and holes generated by photocatalysts.

Acknowledgment. This work was partially supported by the Global Environment Research Fund from the Japanese Government. The authors thank Dr. Defa Wang and Dr. Guoqiang Li for their TEM and SEM analyses. The authors are grateful to Drs. Shinji Itoh, Hitoshi Yamaguchi, and Yukari Ishikawa of Materials Analysis Station for their elemental analyses.

Supporting Information Available: Schematic crystal structures and Raman spectra of $NaLaSrNb_2NiO_9$ and $CsSrLaNb_2NiO_9$ (PDF). This material is available free of charge via the Internet at http://pubs.acs.org.